Importance of the Atmosphere on The Mechanisms and Kinetics of Reactions between Silica and Solid Sodium Carbonate

J Grynberg, E Gouillart, M.-H Chopinet, Michael-J. Toplis

Importance of the atmosphere on the mechanisms and kinetics of reactions between silica and solid sodium carbonate

J. Grynberg,[1] E. Gouillart,[1] M.-H. Chopinet,[1] and M. J. Toplis[2]

[1] *Surface du Verre et Interfaces, UMR 125 CNRS/Saint-Gobain, 93303 Aubervilliers, France*
[2] *IRAP (UMR 5277, CNRS/University of Toulouse III), Observatoire Midi Pyrénées, 14, Ave. E. Belin, 31400, Toulouse, France.*

Using thermogravimetric analysis, the reaction kinetics between powders of silica (SiO_2) and sodium carbonate (Na_2CO_3) are investigated below the melting point of sodium carbonate, under different atmospheres. These experiments show that the reaction kinetics critically depend on the partial pressure of CO_2 in the surrounding atmosphere. Under a flow of nitrogen, the reaction rate is constant with time and follows an Arrhenian law, with a weak influence of the grain sizes of the two reactants. Under a flow of carbon dioxide, the reaction rate is found to be much slower, to have non-linear time dependence and to have a weaker temperature dependence. The influence of grain-size is also found to be more significant in this case. Two different reaction mechanisms between silica and sodium carbonate may account for these results: (i) sodium carbonate dissociates at a rate depending on the partial pressure of CO_2, releasing sodium to the vapor, that may then react with the surface of silica grains; or (ii) silica and sodium carbonate grains react at granular contacts between individual grains. A quantitative equation is proposed that accounts for the influence of temperature, p_{CO_2} and grain size on the reaction rate between silica and sodium carbonate.

I. INTRODUCTION

The system sodium carbonate - silica is one of the simplest possible from which a silicate melt may be produced at temperatures less than 1000° C. In addition, grains of silica and sodium carbonate are among the principal constituents used in the window- or bottle-glass industry.

The reaction kinetics between sodium carbonate and silica powders have been extensively studied [1–7], using various techniques such as thermogravimetric analysis [2, 5], in-situ X-ray diffraction [8], or in-situ ^{23}Na NMR [9]. Reactions are known to be accelerated above the melting point of sodium carbonate at 865° C, when the molten carbonate rapidly wets silica grains [7]. However, reactions may also occur below the melting point of sodium carbonate, either to form crystalline Na_2SiO_3 or $Na_2Si_2O_5$, or even a silicate melt given that the eutectic of the $SiO_2 - Na_2O$ binary is at 785° C [10, 11]. Quantification of the mineralogy and spatial distribution of reaction products is of primary interest, as these factors will influence the evolution of the system at higher temperatures.

There is general agreement [7, 9, 12] that reaction between silica and solid sodium carbonate first produces crystalline Na_2SiO_3:

$$Na_2CO_3 + SiO_2 \rightarrow Na_2SiO_3 + CO_2. \quad (1)$$

However, different authors used different grain sizes, atmospheres or bulk composition, making results on reaction kinetics difficult to compare: published reaction rates at 800° C [2, 8, 13] differ by one order of magnitude. Furthermore, activation energies ranging from 100 kJ.mol^{-1} [6] to 490 kJ.mol^{-1} [13] have been described. Finally, previous studies [4, 11, 14] noticed that reaction rates typically decrease when the sample size increases; this effect was attributed to differences in the partial pressure of CO_2 but the literature shows no example of controlled experiments that tested this hypothesis.

In this work, the reaction kinetics of $SiO_2 - Na_2CO_3$ are revisited, with emphasis being placed on the effect of CO_2 partial pressure. Isothermal thermogravimetric analyses (TGA) are used to measure reaction kinetics as a function of time, for two different atmospheres. Our main result is the identification of two different reaction mechanisms between SiO_2 and Na_2CO_3. In the first, decomposition of sodium carbonate leads to the production of a sodium-containing vapor that reacts with the surface of silica grains that are in the vicinity, but not necessarily adjacent. In the second, reaction occurs at physical contacts between adjacent grains of sodium carbonate and silica. The nature of the dominant mechanism is found to depend on several parameters, in particular the partial pressure of CO_2 and the temperature, but also on grain size.

II. EXPERIMENTAL METHODS

a. Raw materials - Roncevaux silica sand (99.8% silica, 0.05%Al_2O_3, 0.03%CaO, 0.03%Fe_2O_3, 0.01%K_2O 0.02%TiO_2) and Solvay sodium carbonate have been used as starting products. We use industrial-grade (instead of reagent-grade) raw materials because we aim at characterizing reaction kinetics relevant for industrial processes (in particular, with grain sizes close to that used in industry). Sodium carbonate grains have an important micro-porosity. Grains of both carbonate and silica were sieved in three different size bins: 100-160 μm (small - S), 200-250 μm (medium - M) and 400-500 μm (coarse - C). The average size of silica grains used in the float glass industry is close to our medium bin-size. Raw materials were dried at 110° C for several hours before the experiments. All experiments use the same relative

weight proportions of the two reactants: 64% SiO_2 and 36% Na_2CO_3 (corresponding to a final glass composition of 75% SiO_2 and 25% Na_2O). Compared to industrial soda-lime silica glass, this amounts to replacing the fraction of calcium carbonate by sodium carbonate. Mixtures were made from these sieved materials, each mixture denoted by two letters, the first corresponding to the size of silica grains and the second to that of sodium carbonate grains. For example, M-S corresponds to medium silica grains and small sodium carbonate grains.

b. Thermal analyses - Two different thermogravimetric instruments have been used: a Netzsch STA 449C apparatus equipped with an electronic microbalance, operating under a flow of nitrogen, and a Netzsch STA 409C apparatus equipped with a mechanical balance, that operates under a flow of CO_2. A flow rate of 10 mL/min was used. We choose to perform *isothermal* thermogravimetric experiments, since the parameters governing the kinetics of reaction (1) would change with time for a non-isothermal treatment. In all experiments, the sample was heated from room temperature to the temperature of interest at a rate of 10K/min. Samples were then held at constant temperature for one hour in the experiments under nitrogen and some experiments under CO_2, and for 24 hours for the remaining experiments under CO_2. Separate blank runs were used for baseline correction. A sample mass of 100 mg was used for all experiments, with the exception of three experiments, for which a much larger sample mass of 1.4 g was used in order to assess the influence of the size of the system, as in [4, 14].

c. Static melting and observations - Complementary experiments on 5-g mixtures $Na_2CO_3 - SiO_2$ were performed, in order to observe the mineralogy and spatial distribution of reaction products after quenching to room temperature. Samples were characterized using either a binocular microscope or with scanning electron microscopy (SEM). For the acquisition of SEM images the samples were first impregnated with epoxy resin, cut vertically, and polished using a water-free lubricant.

III. RESULTS

A. Nitrogen atmosphere

Measured weight loss is assumed to correspond to that of CO_2 according to Eq. (1). Hence, the fraction X of reacted sodium carbonate may be directly deduced from the thermogravimetric results. The variation of X as a function of time is shown in Fig. 1 for experiments performed under nitrogen, for four different pairs of grain sizes (S-M, M-S, M-M, and M-C), and at three different temperatures (750° C, 800° C and 820° C).

For most experiments, a linear variation of X with time is observed, corresponding to a constant reaction rate:

$$X = \alpha t. \tag{2}$$

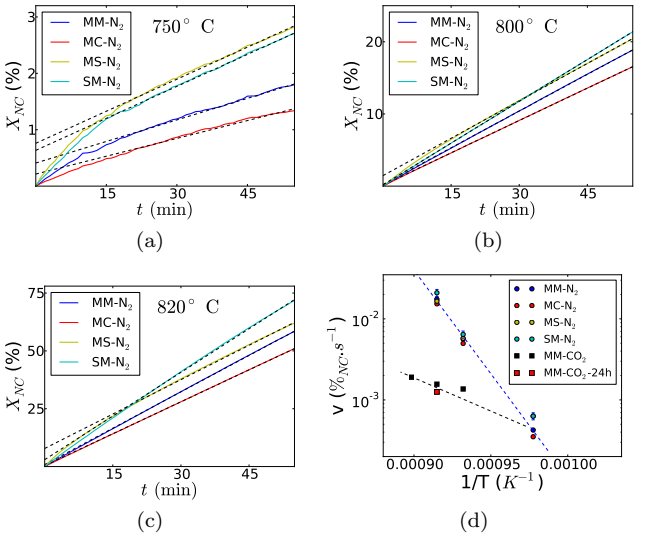

FIG. 1. TGA isothermal treatments (following a 10 K/min ramp to the temperature of interest) under N_2 atmosphere (a-c) Fraction of reacted sodium carbonate as a function of time, at 750° C (a), 800° C (b) and 820° C (c). Mixtures with different grain sizes have been used. (d) The reaction rate as a function of $1/T$, for the experiments of (a-c). The reaction rate is estimated from the weight loss between 15 and 60 min. Circles correspond to the N_2 atmosphere, and black squares to the CO_2 atmosphere.

However, we observe that at 750° C (and to a lesser extent at 800° C) the reaction rate is somewhat faster during the earliest stage of the experiment, before reaching a linear regime. Hence, we define the reaction rate α as the linear regression of data obtained between 15 and 60 min. Reaction rates are shown vs. $1/T$ in Fig. 1 (d). For all grains sizes, an Arrhenian dependence of the reaction rate is observed

$$\alpha(T) = A \exp\left(-\frac{E_1}{RT}\right). \tag{3}$$

The value of the activation energy is similar for all sizes, $E_1 \simeq 490 \pm 30$kJ.mol^{-1}, and comparable to that measured by [13] (443 kJ.mol^{-1}).

The effect of grain size is small, but at fixed temperature experiments performed with smaller grains have a reaction rate that is systematically higher than experiments with larger grains. For the different mixtures, the relative order of the reaction rates is the same for all temperatures. However, the ratio between the fastest and the slowest reaction rates at fixed temperature is less than 2, while the surface area of grains is multiplied by a factor of 16 between small and coarse grains. Therefore, the evolution of the reaction rate is clearly not proportional to the specific surface area of grains of either species.

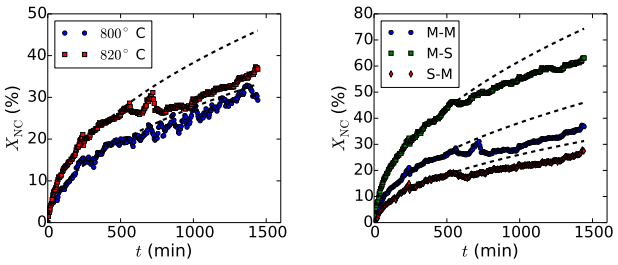

(a) (b)

FIG. 2. Evolution of the reacted fraction X of sodium carbonate vs. time, under CO_2 atmosphere. (a) Thermal treatments of 24 h at 800 and 820°, for the medium grain size. (b) Thermal treatments at 820° C and for different grain sizes.

B. CO_2 atmosphere

Additional TGA experiments were performed under CO_2. For the M-M mixture, thermal treatments for one hour at 750, 800 and 840° C, and for 24-hours at 800 and 820° C were made (see Fig.2 (a)). 24-hour experiments were also performed at 820° C for mixtures M-S and S-M (see Fig.2 (b)).

Comparison of the final extents of reaction after 1 or 24 h shows that heating under a CO_2 atmosphere leads to far less reaction than under nitrogen. To quantitatively compare reaction kinetics under the two atmospheres, a reaction rate was also calculated for the CO_2 experiments as a linear growth rate between 15 and 60 minutes . The reaction rates for the CO_2 experiments defined in this way are shown in Fig. 1 (d): compared to the nitrogen atmosphere, the reaction is slower by more than one order of magnitude. Furthermore, an Arrhenian fit gives a much lower activation energy, $E_2 \simeq 162\text{kJ.mol}^{-1}$.

However, the time-dependence of reacted fraction X under CO_2 is not linear, but can be fitted by a function proportional to the square root of time

$$X = C\sqrt{t}. \tag{4}$$

The coefficient C depends on both temperature and grain size. At constant temperature, the relative ordering of reaction rates as a function of grain size is not the same as that observed under a flow of nitrogen. For example, under CO_2 small sand grains (S-M) lead to a slower reaction rate than medium grains, whereas the opposite is observed under N_2 (Fig. 1 (c)). Under CO_2, the fastest rate is observed for small sodium carbonate grains. At long times (typically after 10 hours), the evolution of X levels-off and is no longer fitted by a square-root function of time, but rather by a (slow) linear evolution.

Overall, given that changing the atmosphere from N_2 to CO_2 leads to very different reactions rates, and that the variation of X as a function of time is different, it appears reasonable to suspect that different reaction mechanisms might be at play in each case.

C. Static melting, air atmosphere

Two static-melting experiments were performed in air atmosphere, using 5 g of the M-M batch. For the first experiment, a lid partially covered the top of the crucible, whereas no lid was used in the second experiment. The samples were heated at 820° C for four hours in two separate experiments. The weight loss was measured after quenching the samples. For the sample with a lid, a reacted fraction X of 38% was computed, whereas the reacted fraction was 83% for the sample without a lid. For comparison, in the TGA experiments the reacted fraction after 4 hours at 820° C is 18% under CO_2 flow (and predicted to be 100% under N_2, from the extrapolation of Fig. 1). Therefore, the reaction rate in air seems to lie in-between those measured under for CO_2 and N_2 atmospheres, with a faster reaction when no lid is present.

SEM images of polished sections of the sample with a lid are shown in Fig. 3 (c-d). Most quartz grains are surrounded by a porous reaction layer, this layer appearing wider close to Na_2CO_3 grains. Using Raman spectroscopy, we observe that this reaction layer is composed of crystalline Na_2SiO_3 and $Na_2Si_2O_5$. On the SEM images, we also observe that the quartz grains have sintered together in many places.

IV. REACTION MECHANISMS

It has been suggested [6] that reaction (1) is controlled by diffusion of alkalis at the surface of silica grains, and later by diffusion through the reacted shell. However, this reaction mechanism alone cannot explain the huge difference between the behavior observed under N_2 and CO_2 atmospheres, in particular the very different time-dependence of reaction extent.

In order to relate the observed differences to reaction mechanisms, we have performed two simple experiments, that aim to highlight to what extent grain-grain contacts are important. In the first experiment, a 5−g $SiO_2-Na_2CO_3$ sample was held for 5 min at 750° C in an air atmosphere. After the treatment, sodium carbonate grains are surrounded by a shell of quartz grains that adhere to the central sodium carbonate grain (Fig. 3 (a)), indicating that reaction has taken place primarily at the contacts between silica and sodium carbonate.

In the second experiment, sodium carbonate and silica were put in physically-separated alumina crucibles, with the silica-containing crucible nested inside the sodium carbonate-containing crucible (inset of Fig. 3 (b)). A lid partially covered the surface of the outer crucible. This sample was held for four hours at 820° C. After quenching, it was observed that the upper layers of sand grains have sintered together (see Fig. 3 (b)). We attribute the mechanical cohesion of these sand grains to a layer of reaction product. Although the reaction layer was too thin to determine its composition using Raman spectroscopy, we believe that it is composed of sodium silicates. In the

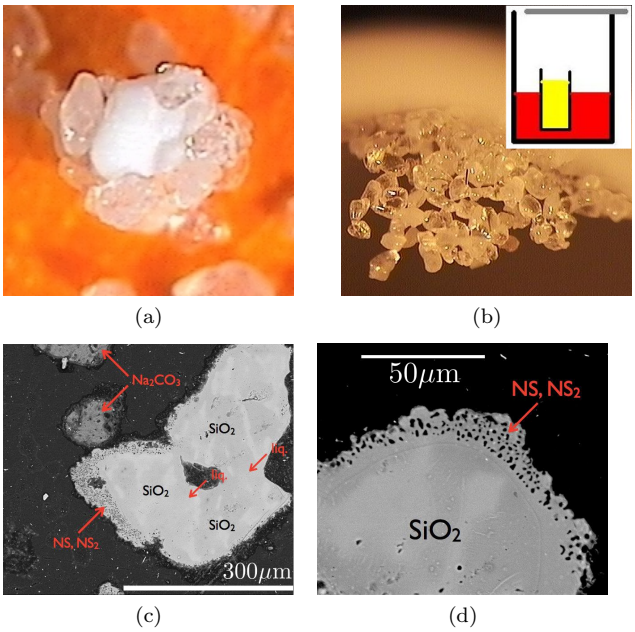

FIG. 3. (a) Grains of quartz (transparent) sticking to a central grain of sodium carbonate (opaque white) after a 4-min thermal treatment at 750°C. A solid-state reaction between the two species is evidenced by the sintering of the grain. The reaction must take place primarily at the contacts between grains, since only quartz grains in contact with sodium carbonate grains sintered. (b) Contact-free experiment. Inset: sketch of the experiment. A crucible filled with quartz grains (yellow) was placed inside a larger crucible filled with sodium carbonate grains (red). Main frame: after 4 hours at 820°C, the quartz grains have sintered together. (c) SEM micrograph of a quenched $SiO_2 - Na_2CO_3$ mixture heated for four hours at 820°C. A porous reaction layer is visible around the quartz grains. (d) Detail of the same micrograph as c).

absence of a physical contact between SiO_2 and Na_2CO_3, the origin of the reaction product is implied to be the decomposition of Na_2CO_3 and the subsequent diffusive transport of a sodium-containing gas, that reacts with the surface of silica grains. This reaction mechanism is discussed in more details in the next section. Surface diffusion along the alumina crucible can be excluded as the primary reaction mechanism, since the sintered grains are found on the upper layers of the sand crucible, and not along its walls. Recent work using in-situ tomography [15] observed that secondary sodium silicates cover a large fraction of the available quartz surface, and not only those regions where quartz and sodium carbonate were in direct contact, providing independent evidence for vapor-phase transport of sodium.

The thermal decomposition of solid sodium carbonate in the absence of any other chemical species has been studied by Preston and Turner [16], using thermogravimetric measurements in dry air as well as in an atmosphere containing water vapor. In their experiments, less than 1% of sodium carbonate was found to have decomposed during a 1-hour thermal treatment at 800° C in dry air, while 5% of sodium carbonate decomposed in an atmosphere of water vapor after 1 hour at 815° C. Using the FactSage Software, we computed the equilibrium constants of the two reactions

$$Na_2CO_3 \rightarrow 2Na_{(g)} + \frac{1}{2}O_{2(g)} + CO_{2(g)} \qquad (5)$$

$$Na_2CO_3 + H_2O_{(g)} \rightarrow 2NaOH_{(g)} + CO_{2(g)}, \qquad (6)$$

to be respectively 4.10^{-22} and 10^{-11} at 820° C. Such weak values explain the slow decomposition rate observed by Preston and Turner.

However, when silica is present, the sodium-bearing gases produced by reaction (5) or (6) may be removed from the vapor to produce Na_2SiO_3:

$$SiO_2 + 2Na + \frac{1}{2}O_2 \rightarrow Na_2SiO_3, \qquad (7)$$

or in the presence of water in the vapor

$$SiO_2 + 2NaOH \rightarrow Na_2SiO_3 + H_2O. \qquad (8)$$

In this case, reaction (5) or (6) are continually displaced to the right, according to Le Chatelier's principle. The decomposition of Na_2CO_3 can thus be accelerated, resulting in the equivalent reaction (1). This mechanism may be used to rationalize the results obtained under a flow of N_2. Most importantly, the activity of sodium-bearing gases in (5) or (6) decreases when p_{CO_2} increases. If the partial pressure of CO_2 is weak (e.g. under a nitrogen atmosphere), the partial pressure of gaseous Na or NaOH at thermodynamic equilibrium is higher than for the case of an atmosphere rich in CO_2. We therefore propose the following expression for the reaction rate:

$$v(p_{CO_2}, T, s) = \frac{A}{p_{CO_2}}\left(1 + \epsilon(s)\right)\exp\left(-\frac{E_1}{RT}\right), \qquad (9)$$

where s is a geometrical parameter accounting for the grain sizes. The factor $1 + \epsilon(s)$ represent the weak dependency of the reaction rate on grain sizes. Since the CO_2 partial pressure can depend on the location inside the sample – under nitrogen flow, one expects p_{CO_2} to be smaller close to the sample surface than at the bottom of the crucible –, the reaction rate of Eq. (9) is local and can vary from one place to another. Our SEM observations confirm that the progress of the reaction always seems to be faster close to the surface of the sample. In addition, three supplementary TGA experiments at 750, 800 and 840° C under N_2 flow, with medium grain sizes M-M and with a larger sample of 1.4 g, show (Fig. 4) that for the two higher temperatures the reaction rate can be fitted with the same activation energy as for the smaller 100-mg samples, but that the reaction rate is significantly smaller for the larger samples. This difference can be attributed to the increased difficulty to evacuate CO_2 for larger samples, a mechanism that had already been

suggested in [11]. At 750° C, the reaction rate is comparable to that of smaller samples, probably because of a combination of the vapor-phase and contact reaction mechanisms.

Under CO_2 flow, the partial pressure of CO_2 is close to 1 everywhere, hence the equilibrium partial pressure of gaseous Na or NaOH is very weak. We deduce that a second reaction mechanism must be at play, that does not depend much on the CO_2 partial pressure. The reaction at intergranular contacts identified in Fig. 3 (a) is probably the second mechanism. It corresponds to reaction (1) that is thermodynamically favored, with an equilibrium constant of 10^3 at 700° C. However, it is kinetically limited by the contact between the two species, explaining why the reaction rate is much slower. With this in mind, we propose the following expression for the reaction rate:

$$v(T,s,t) = \frac{C(s)}{\sqrt{t}} \exp\left(-\frac{E_2}{RT}\right). \qquad (10)$$

The value of the geometrical factor $C(s)$ is discussed in the next section. Since v does not depend on the atmosphere in Eq. (10), we expect that v is constant within the sample, contrary to the case where p_{CO_2} is low.

V. DISCUSSION

A. Effective kinetics

For the vapor-phase reaction (favored by an N_2 atmosphere), it may appear surprising that the reaction rate is constant up to a large value of the reacted fraction (up to 75 %). This observation implies that the same quantity of Na_2O and SiO_2 react per unit time. The porous microstructure of the product layer shown in Fig. 3 (d) may be responsible for this behavior if it consists of open porosity, allowing the gaseous phase to always access the surface of unreacted portions of silica grains. The size of the pores observed in Fig. 3 (d) (a few microns) is indeed much larger than the mean free path of gaseous sodium at 1 bar (¡ 100 nm).

In contrast, the reaction kinetics under CO_2 appear to be diffusion-limited. Different diffusion mechanisms can be invoked to explain the $\sqrt{t}$ scaling for the reaction rate. It is likely that the appearance of the reaction layer creates a barrier through which the sodium has to diffuse, resulting in reaction kinetics that slow down with time. The departure from the square-root dependence observed after 10 hours may correspond to the complete reaction of a fraction of the silica grains.

In our TGA experiments, we have considered extreme cases for the CO_2 partial pressure: $p_{CO_2} \ll 1$ and $p_{CO_2} = 1$. A different reaction mechanism is favored for each of these two cases. In most glass melting experiments, an intermediate value of the CO_2 partial pressure may lead to a combination of the two reaction mechanisms. We therefore propose that the local effective kinetics are described by the sum of (9) and (10):

$$v(p_{CO_2},T,s,t) = \frac{A}{p_{CO_2}}(1+\epsilon(s))\exp\left(-\frac{E_1}{RT}\right) + \frac{C(s)}{\sqrt{t}}\exp\left(-\frac{E_2}{RT}\right). \qquad (11)$$

Because of the different dependence on time and p_{CO_2}, the relative importance of the two mechanisms can vary in space and time. For example, during the initial stages of an experiment, reaction at physical contacts is favored by the large number of initial contacts, explaining why the reaction rate is larger at short times before reaching a constant rate at 750° C under N_2 atmosphere (Fig. 1). Similarly, in a large crucible in a neutral atmosphere, it is expected that the vapor-transport mechanism will be more efficient close to the surface, where the concentration of CO_2 is low, whereas the contact reaction may be more efficient in the bulk, where the CO_2 partial pressure is higher.

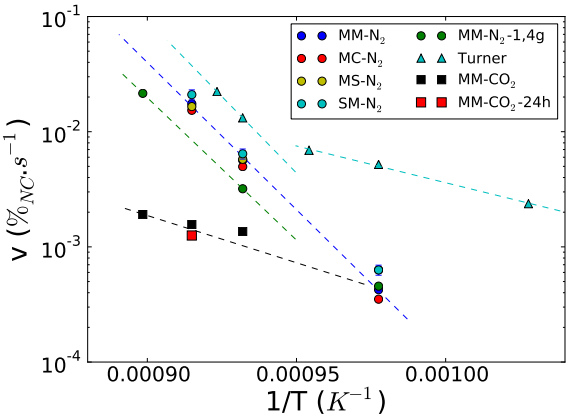

FIG. 4. Arrhenian plot of our experimental results, and comparison with Turner's reaction rates. In addition to the same experimental results as in Fig. 1, we have represented the results obtained by Turner [2] for fine powders (blue triangles). The latter results are well fitted by two Arrhenian curves corresponding to the vapor-phase and the contact reaction mechanisms respectively. In green circles, we have represented the reaction rates obtained for larger samples of 1.4 g.

B. Comparison with results from the literature

The identification of two distinct reaction mechanisms sheds new light on results from the literature, in particular the experiments of Turner [2]. Turner and collaborators performed TGA experiments in air for the same composition as that studied here ($25\%Na_2O - 75\%SiO_2$), using SiO_2 and Na_2CO_3 powders sieved between 80 and 100 μm. The reaction rates of [2], measured during 15 and 60 minutes for different temperatures are reported on Fig. 4. Data at temperatures below 775°C are well fitted by an Arrhenian temperature dependence with an

	M-M	M-S	S-M
C	1.21	1.96	0.80
$Z_{\text{S - NC}}$	2.15	7.26	0.76
$\mathrm{d}\Omega Z_{\text{S - NC}}$	0.29	0.42	0.19

TABLE I. **Correlating reaction rates and geometry:** for the different CO_2 experiments, reaction rate prefactor C, computed number of contacts $Z_{\text{S - NC}}$ between silica and sodium carbonate, and fraction of a sand grain available for reaction with sodium carbonate $\mathrm{d}\Omega Z_{\text{S - NC}}$.

activation energy consistent with that of the contact reaction. In contrast, the two data points corresponding to temperatures above 775°C are fitted with an activation energy consistent with that of the vapor-phase reaction (dashed lines in Fig. 4). The temperature of 775° could therefore be interpreted as the transition from a domain where the contact mechanism dominates to one where vapor transport dominates. The transition temperature is higher for Turner's experiments than in ours because the former used finer powders, for which the contact reaction is favored. The difference in particle size also explains why the value of reaction rate is higher in Turner's experiments, especially in the contact reaction regime.

The more recent results of Dolan and Misture [8] are also in good agreement with our interpretation. [8] observed an activation energy of 157kJ.mol^{-1}, with particles of 100 μm, between 600 and 800°C, consistent with the roles of small particle size and low temperature that are found here to favor the mechanism involving direct grain contacts. On the other hand, experiments performed under partial vacuum by Pole and Taylor [3] and Nandi and Mukerji [13] may be fitted by activation energies of 486 and 444 kJ.mol^{-1}, in good agreement with the vapor-phase mechanism favored at low total pressure and low partial pressure of CO_2.

C. Model for the effective reaction surface

When the contact reaction is the prevailing mechanism (Fig. 2), reaction rate is found to depend significantly on grain sizes. The values of the prefactor $C(s)$ in Eq. (4) are given in Table I and in this subsection, we propose a simple preliminary model to rationalize values of C.

Denoting the radius of silica and sodium carbonate grains as $r_{\mathrm{SiO_2}}$ and $r_{\mathrm{Na_2CO_3}}$ respectively, and assuming that the reaction rate is proportional to the fraction of silica surface in contact with sodium carbonate, the reaction rate can be estimated from

$$C(r_{\mathrm{SiO_2}}, r_{\mathrm{Na_2CO_3}}) \propto n(r_{\mathrm{SiO_2}}) 4\pi r_{\mathrm{SiO_2}}^2 \Omega(r_{\mathrm{SiO_2}}, r_{\mathrm{Na_2CO_3}}), \quad (12)$$

where $n(r_{\mathrm{SiO_2}})$ is the number of quartz grains per unit volume, $n(r_{\mathrm{SiO_2}})4\pi r_{\mathrm{SiO_2}}^2$ is the quartz surface per unit volume, and $\Omega(r_{\mathrm{SiO_2}}, r_{\mathrm{Na_2CO_3}})$ is the surface fraction of a quartz grain that reacts with sodium carbonate. With

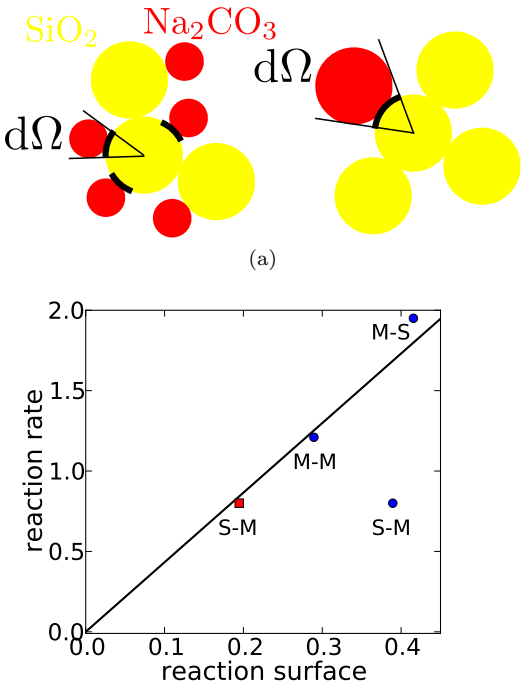

FIG. 5. (a) Sketch of a granular packing. For the contact reaction, the fraction of reactive surface of a silica grain is modeled as the total solid angle that Na_2CO_3 grain(s) occupy on the silica surface. The reaction surface is delineated in black on the quartz surface. For a given composition, small Na_2CO_3 grains (left) are more numerous, but each grain occupies a smaller solid angle $\mathrm{d}\Omega$ on the quartz surface than for medium grains (right). (b) Reaction rate C vs. total reaction surface given by Eq. (13). The red square corresponds to the correction of Eq. (16).

$n(r_{\mathrm{SiO_2}}) \propto r_{\mathrm{SiO_2}}^{-3}$, we obtain

$$C(r_{\mathrm{SiO_2}}, r_{\mathrm{Na_2CO_3}}) \propto r_{\mathrm{SiO_2}}^{-1} \Omega(r_{\mathrm{SiO_2}}, r_{\mathrm{Na_2CO_3}}). \quad (13)$$

For a given contact between one grain of SiO_2 and one grain of Na_2CO_3, the reaction surface may be modeled by the solid angle occupied by Na_2CO_3 on the SiO_2 surface (see Fig. 5 (a)). For one SiO_2 grain, $\Omega(r_{\mathrm{SiO_2}}, r_{\mathrm{Na_2CO_3}})$ is the sum of the solid angles occupied by all its Na_2CO_3 neighbors: $\Omega(r_{\mathrm{SiO_2}}, r_{\mathrm{Na_2CO_3}}) = \sum_i \mathrm{d}\Omega_i$.

In order to compute Ω, one therefore needs to know (i) the average number $Z_{\text{S - NC}}$ of sodium carbonate neighbors of each silica grain, and (ii) the solid angle $\mathrm{d}\Omega$ occupied by a grain of size r_1 on a grain of size r_2:

$$\Omega(r_{\mathrm{SiO_2}}, r_{\mathrm{Na_2CO_3}}) = \mathrm{d}\Omega Z_{\text{S - NC}}. \quad (14)$$

For frictionless grains, the *average* number of touching neighbors Z of a grain is 6. However, large grains will tend to have a larger number of neighbors than small grains. Concerning the solid angle, for a given silica grain the solid angle will be larger as the size of the surrounding carbonate grains increases. Analytical models [17]

have been proposed to describe the geometry of polydisperse granular media. The analytical formula proposed in [17] are used here (as are detailed in the Appendix). The resulting values for the number of contacts Z and the surface fraction Ω are given in Table I. Calculations for silica grains of class corresponding to our medium-class, mixed with small and medium Na_2CO_3 grains shows that the number of contacts is much greater for small grains, but that the solid angle occupied by an individual small grain is also smaller than for a medium grain (see Fig. 5 (a)). For these two experiments (M-M and M-S), the ratio of contact surface areas (Eq. (13)) is approximately that of experimentally determined reaction rates between these two mixtures, as illustrated in Fig. 5 (b). For small silica grains (S-M), $Z_{\text{S - NC}}$ is less than one, and a fraction of the silica grains does not have a single sodium carbonate neighbor. However, the silica surface per unit volume is more important, and the solid angle $d\Omega$ is large. In Fig. 5, it can be seen that the predicted reaction surface per unit volume for the experiment S-M (blue point) is larger than that expected based on the measured rate and the data for the M-M and M-S mixture. One possible explanation for this discrepancy is that the whole solid angle $d\Omega$ is not available for the reaction when the quartz grains are smaller than the Na_2CO_3 grains, since the reaction occurs at the surface of the quartz grains. With this in mind, when the quartz grains are smaller than carbonate grains we propose to replace $d\Omega$ by the equivalent solid angle for Na_2CO_3 grains of the same size as the quartz grains. Making this assumption we find that the experiment S-M verifies relation (13) as well, as shown in Fig. 5 (red square). In light of these results, the following model is proposed to calculate the geometric factor C:

$$C(r_{\text{SiO}_2}, r_{\text{Na}_2\text{CO}_3}) \propto r_{\text{SiO}_2}^{-1} Z \mathrm{d}\tilde{\Omega}(r_{\text{SiO}_2}, r_{\text{Na}_2\text{CO}_3}), \quad (15)$$

$$\mathrm{d}\tilde{\Omega}(r_{\text{SiO}_2}, r_{\text{Na}_2\text{CO}_3}) = \min\left(\mathrm{d}\Omega(r_{\text{SiO}_2}, r_{\text{Na}_2\text{CO}_3}), \mathrm{d}\Omega(r_{\text{SiO}_2}, r_{\text{SiO}_2})\right). \quad (16)$$

While this model provides a promising approach to quantification of reaction rates, experiments with other grain sizes are needed to test the geometric model. It would also be interesting to investigate the extent of the reaction surface between silica and molten sodium carbonate (above the melting point of sodium carbonate): on the one hand, molten sodium carbonate may spread on the quartz surface and increase the reaction surface; but on the other hand, capillary forces may lead to molten sodium carbonate wetting preferentially some quartz grains at the expense of other quartz grains initially in contact with solid sodium carbonate.

D. Conclusions

In conclusion, it seems appropriate to quote W.E.S. Turner, who stated in 1933 [2] "Despite several earlier investigations on the subject of the reaction between sodium carbonate and silica [...], it seemed to us that much remained yet to be learnt about the early stages of the reaction, particularly below the melting point of sodium carbonate". Nevertheless, our results as well as most previous results from the literature can be explained by a combination of the two different reaction mechanisms identified in this article. In summary, when CO_2 can be efficiently removed from a decarbonating mixture, the partial pressure of sodium is large enough so that a vapor-phase reaction dominates. On the other hand, sodium carbonate and silica also react at the contacts between the two species. In this case, the reaction rate is dominated by diffusion through the reacted layer, leading to a reacted fraction proportional to $\sqrt{t}$. In most cases, a combination of the two mechanisms will be observed.

Whereas the mechanism involving vapor transport is sensitive to local variations in p_{CO_2}, the other mechanism is found to be sensitive to the local geometry of grains, and the effective contact surface area between grains of different composition. A model for the effective contact surface area has been proposed, that is shown to account well for our experimental results.

We gratefully acknowledge the help of Catheline Cazako, Nathalie Ferruaud, and Samuel Pierre for the experiments, and fruitful discussions with Cyril Condolf, Pierre Jop, Sophie Papin and William Woelffel.

[1] J.T. Howarth, R.F.R. Sykes, and W.E.S. Turner. A study of the fundamental reactions in the formation of soda-lime-silica glasses. *Sheffield Meeting*, 1931.

[2] J.T. Howarth, W. Maskill, and W.E.S. Turner. The rate of reaction between silica and sodium carbonate at different temperatures and the process of vitrification. *Journal of the Society of Glass Technology*, 1933.

[3] G.R. Pole and N.W. Taylor. Kinetics of solid-phase reactions of certain carbonates with mullite, silica and alumina. *Journal of the American Ceramic Society*, 18(1-12):325–337, 1935.

[4] George Gibsont and Roland Ward. Reactions in solid state: 111, reaction between sodium carbonate and quartz. *Journal of the American Ceramic Society*, 26(7):239–246, 1943.

[5] F.W. Wilburn and C.V. Thomasson. The application of differential thermal analysis and thermogravimetric analysis to the study of reactions between glass-making materials - part 1. the sodium carbonate - silica system. *Journal of the Society of Glass Technology*, 1958.

[6] W.R. Ott. Kinetics and mechanism of the reaction between sodium carbonate and silica. *Ceramurgia Interna-*

tional, 5(1):37–41, 1979.
[7] P. Hrma. Reaction between Sodium Carbonate and Silica Sand at 874° C < T < 1022° C. *Journal of the American Ceramic Society*, 68(6):337–341, June 1985.
[8] Michael D Dolan and Scott T Misture. Kinetics of glass batch reactions. *Glass technology*, 48(2):89–100, 2007.
[9] Aled R Jones, Rudolf Winter, Pierre Florian, and Dominique Massiot. Tracing the reactive melting of glass-forming silicate batches by in situ 23Na NMR. *The journal of physical chemistry. B*, 109(10):4324–32, March 2005.
[10] FC Kracek. The system sodium oxide-silica. *The Journal of Physical Chemistry*, 34(7):1583–1598, 1930.
[11] P Hrma. Batch melting reactions. *Paul, A.: Chemistry of Glasses. Chapman and Hall, London*, pages 157–177, 1999.
[12] Jong-Wan Kim, Yong-Deuk Lee, and Hae-Geon Lee. Decomposition of Na2CO3 by interaction with SiO2 in mold flux of steel continuous casting. *ISIJ international*, 41(2):116–123, 2001.
[13] A. K. Nandi and J. Mukerji. Reaction of silica with Na_2CO_3 and with the eutectic and double carbonate of Na_2CO_3 and $CaCO_3$. *ICG Congres*, 1:177–185, 1986.
[14] T. Moriya and T. Sakaino. On the rate of solid reaction in the Na$_2$CO$_3$-SiO$_2$ system. *Tokyo Inst. Tech. Series B*, 2:13–46, 1955.
[15] E. Gouillart, M.J. Toplis, J. Grynberg, M.-H. Chopinet, E. Sondergard, L. Salvo, M. Suéry, M. Di Michiel, and G. Varoquaux. In-situ synchrotron microtomography reveals multiple reaction pathways during soda-lime glass synthesis. *Journal of the American Ceramic Society*, page 4, January 2012.
[16] E. Preston and W.E.S. Turner. The decomposition of sodium carbonate. *Journal of the Society of Glass Technology*, 1934.
[17] M. Danisch, Y. Jin, and H.A. Makse. Model of random packings of different size balls. *Physical Review E*, 81(5):051303, 2010.

APPENDIX: COMPUTATION OF REACTION SURFACES

For the geometric model of reaction surfaces, we have used the formula derived in Danish et al. [17] for the geometry of a bidisperse packing of grains. The solid angle Ω_{ij} that a ball of radius R_j occupies on a ball of radius R_i can be computed from the geometry only as

$$\Omega_{ij}/2\pi = \int_0^{\arcsin\left(\frac{R_j}{R_i+R_j}\right)} \sin\theta \mathrm{d}\theta = 1-\sqrt{1-\left(\frac{R_j}{R_i+R_j}\right)^2}. \quad (17)$$

Noting x the fraction of grains of species 1, the average fraction of occupied surface of a grain of species i is then

$$\Omega_i^{\mathrm{occ}} = x\Omega_{i1} + (1-x)\Omega_{i2}. \quad (18)$$

Noting Z the average coordination number in the packing ($Z = 6$ for frictionless grains), Z_i the average coordination number of grains of species i, and Z_{ij} the average number of neighbors j for a grain i, Danish et al. derive the following relations:

$$Z_{11} = \frac{Z_1^2 x}{Z}, \quad Z_{12} = \frac{Z_1 Z_2 (1-x)}{Z},$$
$$Z_{21} = \frac{Z_1 Z_2 x}{Z}, \quad Z_{22} = \frac{Z_2^2 (1-x)}{Z}; \quad (19)$$

$$Z_1 = \frac{Z}{x + (1-x)\frac{\Omega_1^{\mathrm{occ}}}{\Omega_2^{\mathrm{occ}}}},\ Z_2 = \frac{Z}{x\frac{\Omega_2^{\mathrm{occ}}}{\Omega_1^{\mathrm{occ}}} + (1-x)}, \quad (20)$$

from which contacts statistics of Table 1 are derived.